Article

Research and Application of Interferogram Acquisition Method for Ground-Based Fourier-Transform Infrared Greenhouse Gas Spectrometer

Yasong Deng [1,2], **Liang Xu** [1,*], **Ling Jin** [1], **Yongfeng Sun** [1], **Lei Zhang** [1,2], **Jianguo Liu** [1] **and Wenqing Liu** [1]

[1] Key Laboratory of Environmental Optics and Technology, Anhui Institute of Optics and Fine Mechanics, Hefei Institutes of Physical Science, Chinese Academy of Sciences, Hefei 230031, China; ysdeng@aiofm.ac.cn (Y.D.)

[2] School of Environmental Science and Optoelectronic Technology, University of Science and Technology of China, Hefei 230026, China

[*] Correspondence: xuliang@aiofm.ac.cn

Abstract: A high-performance data acquisition and processing system within a spectrometer provides a powerful guarantee for obtaining high-precision data in ground-based Fourier-transform infrared greenhouse-gas spectroscopy. Addressing the challenge of accurate interferogram sampling in Fourier-transform spectroscopy, a dual-channel interferogram acquisition method was designed. Dual-channel analog-to-digital converters, acquiring interferograms at different gains, enable high dynamic range and high-resolution acquisition of infrared interferometric signals; the analog-to-digital converter channel of low-gain interferograms mainly captures data near the zero-optical-range-difference spike, and the analog-to-digital converter channel of high-gain interferograms mainly acquires the weak signals from the two flanks. The simulation results, circuit design, and correction method between the two channels of the method are given. Finally, in the ground-based Fourier-transform infrared greenhouse-gas spectrometer for experimental applications, the experiment shows that under the same measurement conditions, the carbon dioxide column concentration-measurement accuracy is improved by 2.096 times, and the dual-channel interferometric data acquisition method can significantly enhance the data retrieval accuracy.

Keywords: Fourier-transform infrared spectroscopy; interferogram acquisition; greenhouse gases; carbon dioxide

1. Introduction

Ground-based Fourier-transform infrared (FTIR) measurements are available at various locations around the world for determining atmospheric trace gas concentrations and investigating climate change [1–3]. Fourier-transform spectrometers have become the tool of choice in the field of high-performance spectral analysis because of their excellent performance in simultaneous signal processing, high-throughput, high resolution, and high wavelength accuracy [4,5]. As the core of FTIR spectroscopy system, the Michelson interferometer is used to obtain spectra by measuring interferograms and performing Fourier transforms to characterize the morphology and quantify the substances [6]. However, sampling errors in interferograms are an important source of spectral noise in conventional sampling methods [7]. Any error in the sampling process will have a significant impact on the spectral performance, which is manifested in the appearance of spectral artifacts, shift in the spectral position, and increase in the spectral noise [8]. These effects not only

reduce the clarity and resolution of the spectrum, but also seriously interfere with the accuracy and reliability of spectral analysis [9]. Therefore, in the application of the FTIR spectrometer, how to accurately control the sampling process of the interferogram and reduce the sampling error is key to improving the spectral performance and ensuring the accuracy of the spectral analysis. Furthermore, the results also highlight new challenges and requirements for the design and optimization of spectroscopic instruments.

Inaccurate sampling of the interferogram may result in the generation of another type of noise in the spectrum, known as quantization or digitization noise [10]. The source of digitization noise is illustrated in Figure 1, where a discrepancy between the sampled and true values of the waveform is evident. This discrepancy corresponds to noise in the signal and will translate into spectral noise. In Fourier-transform spectroscopy, an analog time-domain signal is sampled at equal intervals and then subjected to a discrete Fourier transform to obtain a discrete frequency-domain spectrum. Even when the time-domain analog signal is noiseless, rounding errors during the sampling process introduce quantization "noise" [11].
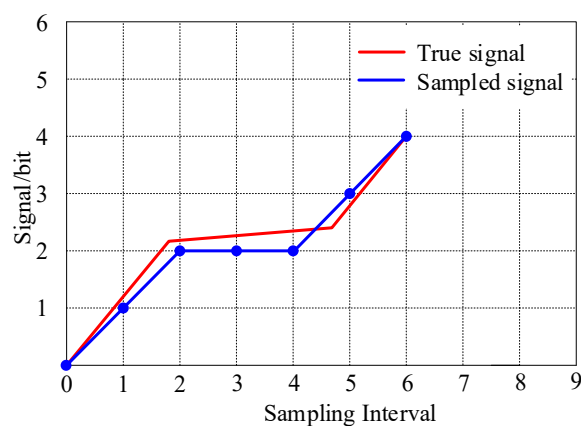

Figure 1. Sources of digitized noise. The difference between the actual signal and the sampled signal at each data point is demonstrated. This error can be approximately considered equivalent to the peak-to-peak detector noise of 1/2 bit.

Traditional interferogram data acquisition methods primarily rely on single-channel analog-to-digital converters (ADCs). Although this method fulfills basic acquisition needs to a certain extent, its inherent limitations, such as sampling errors, quantization noise, and limited dynamic range, severely hinder the further enhancement of spectral analysis performance [12]. These limitations are particularly evident when dealing with spectral analysis of wide spectral ranges or complex substances. To address the issue of interferogram sampling, researchers have proposed various improved methods from different fields. One study [13] established a theoretical model linking the relative error of spectral measurement to the deviation of sampling points for the analysis and correction of spectrometer sampling errors based on Fourier inverse-transform and error-analysis methods. One study [7] introduced analog and digital amplitude and phase components as compensated acquisition systems to mitigate spectral noise caused by sampling errors. However, excessive compensation also increases system uncertainty.

To overcome these challenges, researchers have begun exploring the application of dual-channel ADCs in interferogram data acquisition. By acquiring interferometric signals simultaneously from two or more channels, the dual-channel analog-to-digital converter (ADC) technique not only effectively increases the sampling rate and resolution, but also significantly reduces quantization noise, thereby improving the overall quality of spectral data. Furthermore, the dual-channel acquisition strategy aids in achieving more accurate

spectral recovery and reducing the occurrence of spectral position shifts and spectral ghosting, which is crucial for enhancing the accuracy and reliability of spectral analysis. One study [14] designed an acquisition system based on segmented gain control for an FTIR spectrometer, where the infrared interferometric signal peaks at zero optical-path difference (ZPD). The signal attenuation outside the ZPD is similar to that of noise, exhibiting a large overall dynamic range. The acquisition system employs segmented gain control, utilizing a programmed gain amplifier module and an Field Programmable Gate Array (FPGA)-based multiplexed acquisition module to acquire infrared interference signals with a high dynamic range. Simulated interference signal tests demonstrate that this design enhances weak signal acquisition outside the ZPD, improves system dynamic range, and accurately restores the real spectrum.

Regarding the above issue, the interferogram may exhibit an abnormally high signal-to-noise ratio (SNR) due to its inherent properties, particularly at zero delay. As the interferogram region moves away from the ZPD, the phase difference of the waves increases, weakening the amplitude superposition effect and resulting in a gradual decrease in signal strength. Simultaneously, background noise becomes more prominent, causing the SNR of the interferogram region away from the zero-delay point to decrease significantly. In this paper, we propose a dual-channel interferometric data-acquisition method that simultaneously acquires interferometric data near and far from the zero-delay point. This method leverages information from the high-SNR region, while reducing the interference from the low-SNR region on overall measurement results.

In Section 2, we present the theory and specific implementation steps of the dual-channel interferometric data-acquisition method. In Section 3, we conduct a simulation analysis of the acquisition method and present the hardware design of the acquisition circuit based on MATLAB(2016b) software. Additionally, we provide methods for calibrating and correcting errors between the dual channels. In Section 4, we apply the proposed dual-channel interferometric data-acquisition method to a ground-based greenhouse-gas spectrometer to obtain observation results for carbon dioxide (CO_2) column concentration. Finally, some conclusions are given in Section 5.

2. Dual-Channel Interferometric Data-Acquisition Methods

In order to more thoroughly sample the signals on both flanks of the IR interferogram, more and more instruments are using sampling of ADC gain switching to increase the dynamic range of interferogram sampling. As shown in Figure 2, the gain is switched once for $g = 2^N$ (N is an integer) data points on both sides of the ZPD position, and the gain at positions away from the ZPD is usually amplified by more than 8 times that at the ZPD position. Therefore, the principal ZPD position data are amplified to obtain more accurate sampling.

In an FTIR spectrometer, the accuracy of the ADC must exceed the dynamic range in order to discriminate the smallest signal elements in the range. When the digital voltage signal or the ADC's dynamic range is insufficient, certain sharp spectral signals in the interferogram may become blurred, resulting in the useful interferogram signals being obscured by noise. In cases where the acquisition ADC's accuracy is limited, in order to improve the accuracy of the weak signals in the two wings of the interferogram, according to the characteristics of the interferogram, the design employs a segmented variable-gain method: a low gain is used at the zero optical-path difference spike, and, as the signal diminishes, it switches to a high gain, which amplifies the small signals in the two wings, thereby enhancing quantization efficiency during sampling and improving sampling accuracy. When the gain is applied, the signal is quantized and captured by the ADC, resulting in an equivalent increase in resolution by g bits.
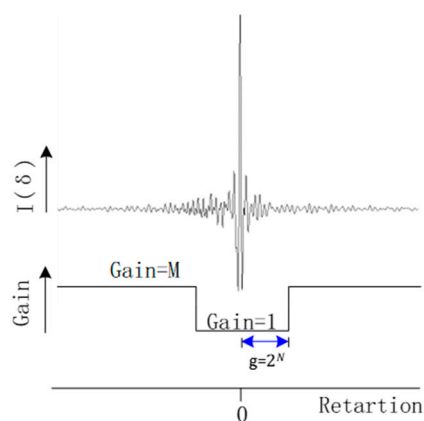
Figure 2. Schematic diagram of amplified gain range.

When the gain is minimized, the ADC's dynamic range must be at least as large as the interferogram's dynamic range. When variable gain amplification is performed on small signals, the amplified signal intensity should not exceed the intensity of the zero optical-range difference spike, lest it exceed the ADC's dynamic range. Maximum gain can be applied to signals whose intensity is close to the RMS value. However, gain switching introduces complexities in precise synchronization control and may cause data fluctuations due to unstable control of the gain switching process. Therefore, a dual-channel interferometric data acquisition method is designed to achieve high-accuracy interferogram sampling with a high dynamic range.

The dual-channel interferometric data acquisition method primarily consists of dual-channel ADC acquisition and low-delay square-wave triggering. Moreover, the system block diagram illustrating this method is shown in Figure 3. Based on the working characteristics of the interferometer, the gain adjustment process involves dividing the detection signal into two channels, firstly, and then the signals of each channel are amplified with different gains, respectively, while the two channels remain parallel and independent of each other.
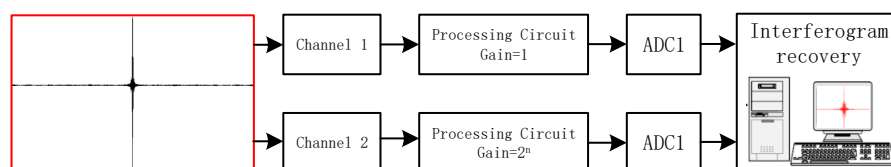

Figure 3. Schematic of data acquisition process.

After obtaining two channels of interferometric data, it is also necessary to carry out the normal calibration procedure on the interferograms. Using open sources or spectrometers for vehicle applications, the interferograms will show jitter, affecting the recovery of the interferograms. Each data point on the calibrated two-channel interferogram needs to be divided by the corresponding gain magnification, so as to convert the entire interferogram to the same effective gain before the Fourier transform. This process of recovering the true interferometric signal is also referred to as data synthesis. The details of the data synthesis process, which combines two channels of data into a single set through splicing, are given in Section 3.1.

3. Simulation Analysis and Circuit Design

3.1. Simulation Experiments and Analysis

A dual-channel 16-bit ADC acquisition card with a dynamic range of -0.1 to 0.1 was simulated using MATLAB software (R2016b). A raw interferogram, used as the data

input for ADC channel one, was processed without magnification (Figure 4a). The same interferogram, magnified by a factor of 8, served as the data input for ADC channel two (Figure 4b). Figure 4c,d show the quantization results of the two channels, respectively. Since channel two is primarily designed to capture small signals from the interferogram wings, gain amplification is often applied, but the amplified signal intensity must not exceed the zero optical-range difference spike intensity, otherwise, it will exceed the ADC's dynamic range. The center region of the ZPD in channel two's interferogram approaches the upper limit of this dynamic range.
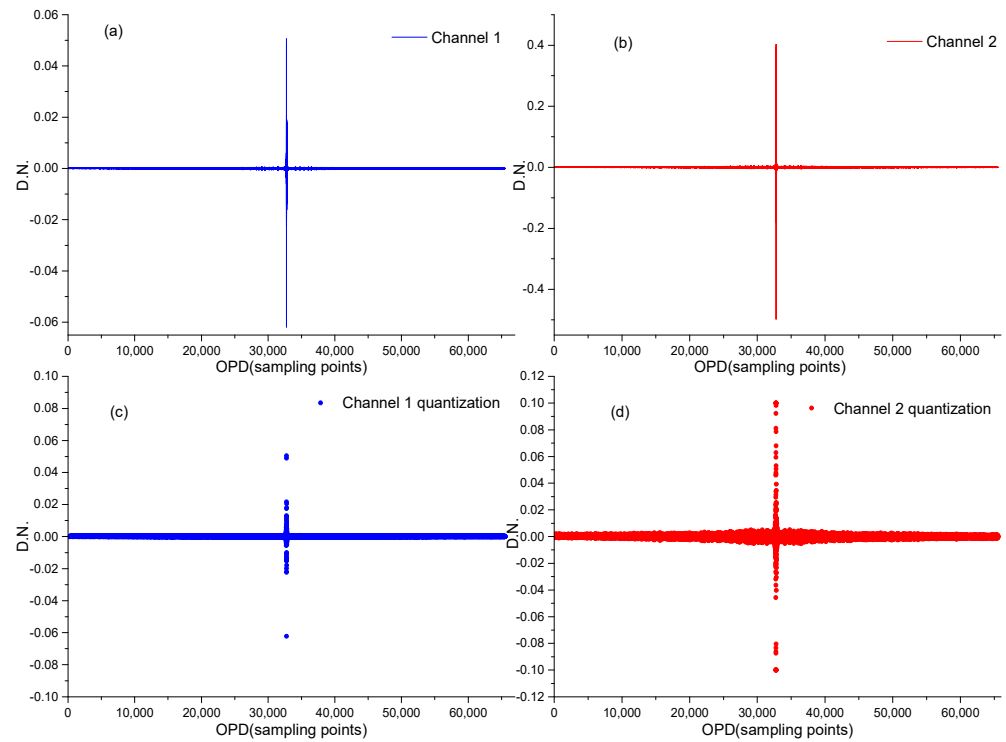

Figure 4. Dual-channel acquisition of interferograms: (**a**) interferograms at the input of ADC channel 1; (**b**) interferograms at the input of ADC channel 2; (**c**) quantization of interferograms by ADC channel 1; (**d**) quantization of interferograms by ADC channel 2.

The zero-delay coefficient, g, between intervals of gain switching is given by $g = 2^N$, where N is an integer; thus, g = 2, 4, 8, etc. All data points on the calibrated two-channel interferogram must be divided by their corresponding gain amplification to convert the entire interferogram to a uniform effective gain, prior to performing the Fourier transform (as shown in Figure 5).

After recovering the interferograms, we used the standard interferogram data processing and spectral conversion process to successfully obtain the corrected spectral data (shown in Figure 6a). In order to analyze the effect of the solar tracking system on the quality of the FTIR spectra, the performance of the infrared instrument is usually evaluated using the instrumental R_{SNR}, expressed as Equation (1), and the instrumental signal-to-noise ratio analysis is chosen to be from 6000 cm^{-1} to 6200 cm^{-1} [15]; the R_{SNR} of the reconstructed spectra of the original single-channel acquisition and the dual-channel acquisition are calculated to be, respectively, 2.128×10^3:1 and 2.613×10^3:1, and the R_{SNR} was improved by a factor of 1.23 (shown in Figure 6b).

$$R_{SNR} = \frac{100}{N} \tag{1}$$

where N is the peak noise value measured by the transmittance representation.
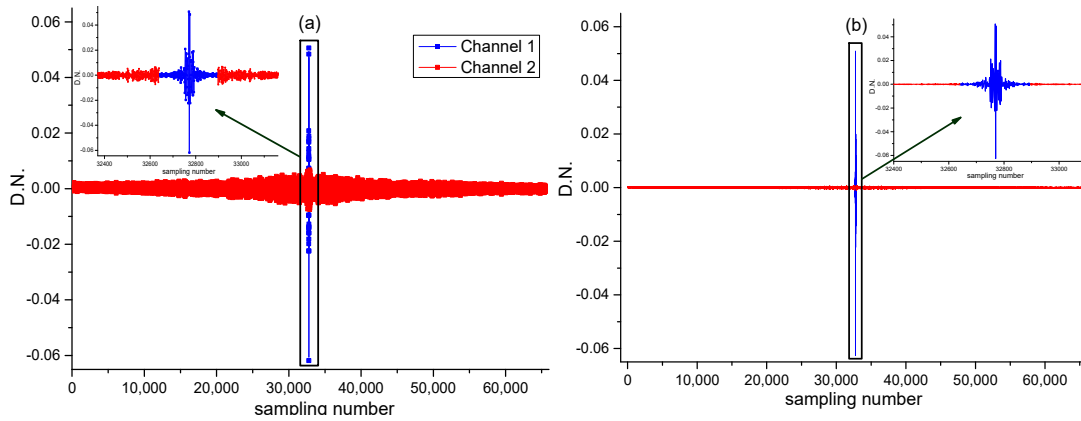
Figure 5. Dual-channel acquisition of interferogram recovery results: (**a**) acquisition of two channels of raw data; (**b**) the recovered interferogram.
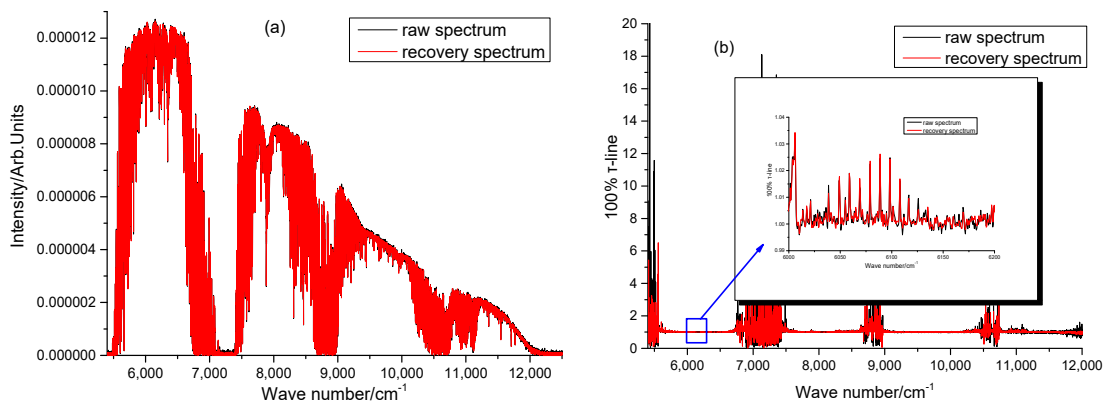

Figure 6. Analysis of the recovered spectral results: (**a**) The spectral profiles obtained by the two methods are consistent; (**b**) 100% of the τ-lines falling within the spectral range of 6000 to approximately 6200 cm^{-1}.

3.2. Hardware Design and Analysis

Matlab simulation experiments verify the feasibility of the proposed dual-channel interferometric data acquisition method, and demonstrate an improvement in spectral data quality. This section will focus on the design and analysis of several key circuit modules essential for the hardware implementation of the method, including the power supply circuit, the amplification and detection circuit for the detector signal, and the dual-channel acquisition and processing circuit.

(1) Low-noise power supply circuit design

The design of the power supply plays a crucial role in operational amplification circuits. It can directly affect the stability, performance of the circuit, and the adaptability of the application scenario. In circuit design, most often, regulated power supplies are used. The function of a regulated power supply is to obtain a stable direct current (DC) voltage from a slightly unstable power source. The main technical requirements for a regulated power supply are accuracy and stability. The power supply is also usually required to have an appropriate current output capability (preferably less than milliamps, depending on the application). There are usually two types of regulated power supplies: linear regulated-power supplies and switching regulated-power supplies, which tend to suffer from more serious noise disturbances. Therefore, we choose the purer linear regulated-power supply.

The design circuit is shown in Figure 7, with a ±15 V power supply capacity. The power supply output uses the LT1963 and LT1175 voltage regulator modules from analog

devices [16], which feature very low operating current, rapid transient response, and low output noise characteristics.
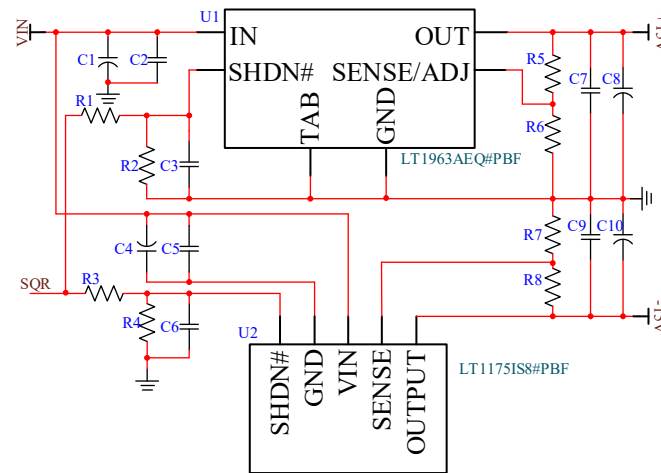

Figure 7. Power supply-circuit design schematic.

(2) Signal-detection and amplification circuit design

The solar-spectral ground-based FTIR system utilizes a high-performance InGaAs detector that operates within the spectral range of 0.7 μm to 1.8 μm. It is characterized by a fast rise time, stable temperature response, wide dynamic range, and high sensitivity. To enhance the performance, particularly the temperature stability of the response near the cutoff wavelength, it is necessary to utilize it in conjunction with a thermoelectrically cooled temperature controller. The equivalent circuit of an InGaAs photodiode, depicted in Figure 8, represents a photon-generating current source accompanied by a shunt resistor (R_D), a shunt capacitor (C_D), and a series resistor (R_S). The value of R_S is negligible compared to R_D, except at high power levels (exceeding 10 mW). The InGaAs photodiode generates current across the PN junction when photons with sufficient energy are absorbed in its active region.
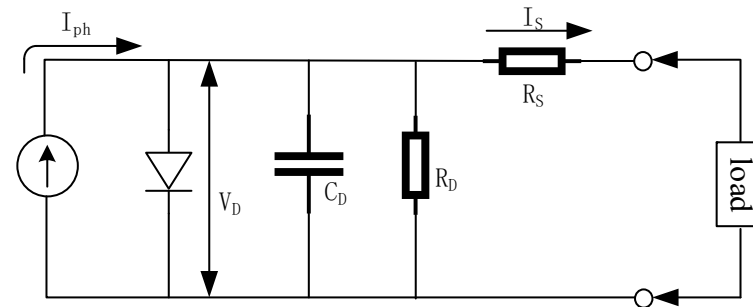

Figure 8. InGaAs photodiode equivalent circuit.

The infrared signal originally detected by the detector is relatively weak, and the design of the amplification and detection circuit must meet the technical specifications for low-noise and high-gain amplification. In Figure 7, the first stage of amplification is a negative feedback operational amplifier (op-amp). The feedback circuit converts the detector's output current to a voltage, while the op-amp maintains the detector at a near-zero-volt bias to minimize noise. However, there is a DC offset current, also known as the "dark current" of the detector circuit. This dark current is a function of the preamplifier's

input bias current (I_b), the preamplifier's input offset voltage (V_{os}), and the detector's shunt resistor (R_D). The total "dark current" can be expressed by Equation (2).

$$I_D = I_b + \frac{V_{os}}{R_D} \tag{2}$$

Therefore, choosing the right operational amplifier is crucial for reducing preamplifier noise and achieving optimal system bandwidth. For a high R_D detector, select a preamplifier with a low bias current; for a low R_D detector, choose one with a low output offset voltage.

Here, we utilize the officially recommended Quest Components model OPA111, a high-precision, low-noise differential amplifier (with a maximum noise of 8 nV/$\sqrt{\text{Hz}}$ at 10 kHz), featuring low drift (with a maximum temperature drift of 1 μV/°C) and a high common-mode rejection ratio of 100 dB. The maximum input bias current is 1 pA, and the minimum open-loop gain is 120 dB.

To reduce circuit noise while maintaining the signal's gain bandwidth, the first-stage op-amp circuit must satisfy the conditions C1 = C2 and R2 × C2 = R4 × C7. The second-stage circuit provides voltage amplification and is capable of DC-coupled input and output for the IR signal (Figure 9).
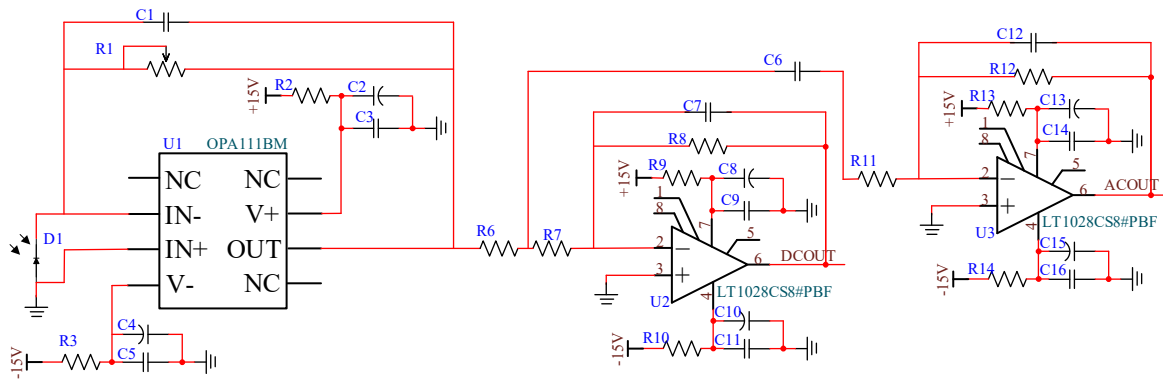

Figure 9. Interference signal amplification-detection circuit schematic.

(3) Dual-channel acquisition and processing circuit design

Based on the proposed dual-channel interferometric data acquisition method, the gain adjustment of the detection signal is realized, building upon the previous design of the power supply circuit and the signal detection and amplification circuit. Specifically, the detection signal is divided into multiple channels, each of which is amplified with a different gain. These channels are parallel to, and independent of, each other. The advantage of this approach is that each channel operates in parallel, eliminating the need for synchronization control.

Following the aforementioned infrared interferogram segmentation and gain design, the interferogram is split into two parts with different gains, necessitating two channels for amplification and collection. This setup avoids the complexity of precise synchronization control.

In response to the requirements of the circuit design, we have designed the two-stage synchronization circuit shown in Figure 10. The variation in gain is primarily determined by R3 and R9. To enhance the stability and reliability of the circuit, we have incorporated a T-capacitor filter to fulfill the filtering function of the method.
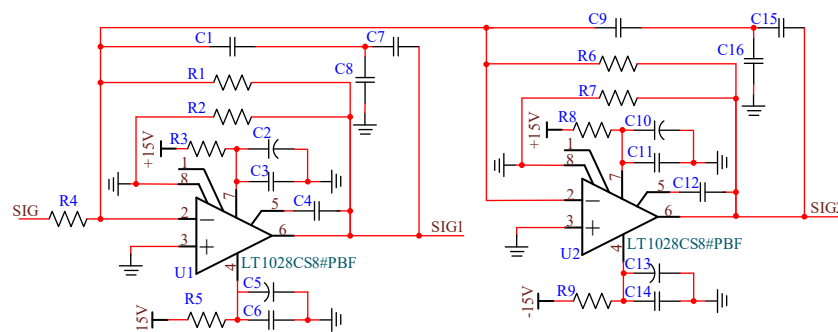
Figure 10. Schematic diagram of two-stage gain synchronous amplifier circuit.

3.3. Calibration and Correction of Channel Errors

When an ADC acquires an analog signal and converts it into a digital signal, it generates certain errors, due to various reasons such as hardware limitations, environmental factors, and circuit design imperfections. These errors may encompass nonlinearity errors, gain errors, and offset errors. Through software correction, these errors can be mitigated to a certain extent, thereby improving the acquisition accuracy of the ADC. The specific correction steps are as follows:

a. Access a known zero-voltage signal at the input of the ADC, read the output value of the ADC (which represents the zero offset of the ADC), and subtract this zero offset from subsequent ADC output values to achieve zero calibration.

b. Apply a known full-scale voltage signal to the input of the ADC, and read the ADC's output value (which corresponds to the ADC's output at full-scale voltage). The theoretical output value of the ADC at full-scale voltage should equal the reference voltage. Adjust the actual ADC output value to match the theoretical value proportionally through software programming, thereby achieving full-scale calibration.

c. Measure the ADC's output value at several known input voltage points. Based on the measured output values and the corresponding input voltage values, calculate the offset and gain factor for the ADC in each voltage range. In the software, create a look-up table to store the offsets and gain coefficients for each voltage range. During data acquisition, retrieve the corresponding offsets and gain coefficients from the look-up table based on the input voltage range, and use them to correct the ADC's output value.

4. Applications and Analysis

4.1. Experimental Instruments

In the experimental application, the self-developed AG-FTIR-GH2000 near-infrared solar absorption spectrometer was utilized to determine the column concentration of CO_2. To attain a retrieval accuracy exceeding 0.5%, the spectrometer incorporated high-precision dynamic collimated interferometry. Additionally, we utilized silver-plated optics, a calcium fluoride beamsplitter, and an InGaAs detector to achieve a spectral range spanning from 5400 to 12,800 cm^{-1}, with a resolution of 0.5 cm^{-1} and a scanning speed of 100 kHz for solar absorption spectra. The sun tracker, which integrates both an image sensor and a position sensing detector (PSD), directs sunlight into the spectrometer's entrance. The image sensor captures deviations in the sun's exact position at a rate of 3 Hz, while the position detector automatically searches for the sun's position at a rate of 100 Hz whenever the image is lost (Figure 11).
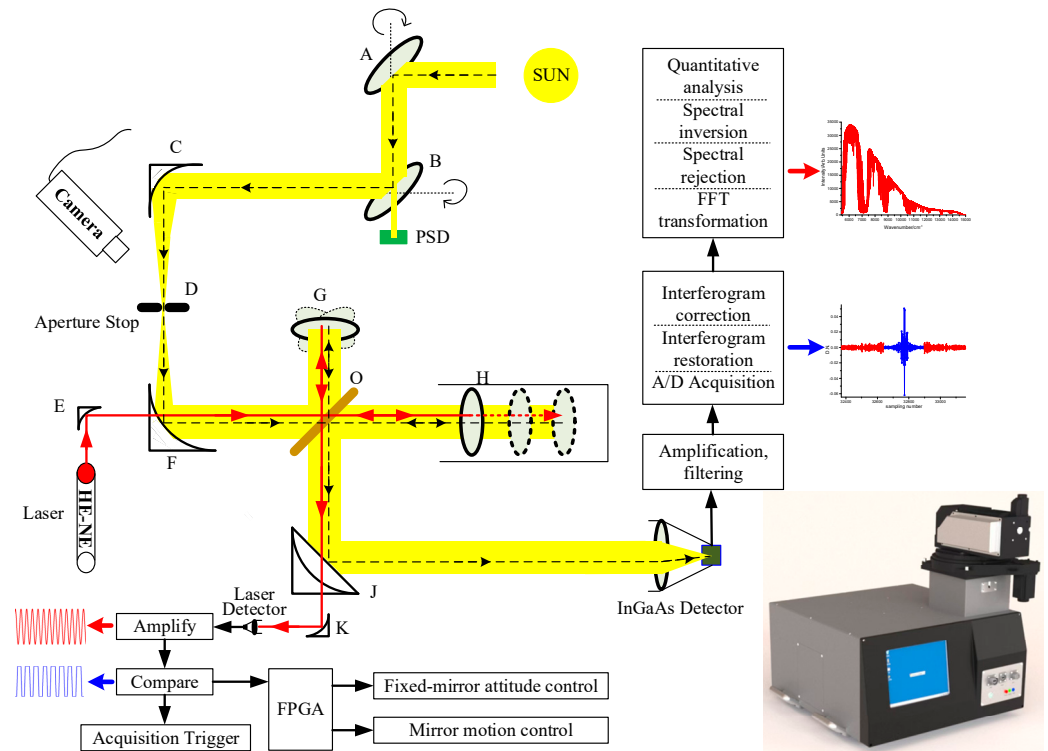
Figure 11. Solar spectrum ground-based FTIR spectrometer.

The sun tracker primarily serves as a light-source introduction system for the FTIR spectrometer. Sunlight traverses reflector A (which adjusts according to the sun's altitude angle) and reflector B (which adjusts according to the sun's azimuth angle). Reflector B features a 5 mm diameter through-hole at its center, allowing sunlight to pass through and illuminate the position detector. This detector, in turn, drives the tracking system via the controller to achieve coarse tracking of the sun's movement. The sunlight is then focused through the central field of view of a diaphragm by parabolic mirror C. Notably, the center of the diaphragm is positioned 2 cm away from the focal point. The diaphragm offers two primary advantages. Firstly, it ensures that the FTIR's resolution meets the design requirements by defining the interferometer's field of view. Secondly, any positional deviation in the beam passing through the small aperture is captured and analyzed in real-time by a camera. Based on this analysis, the controller adjusts the tracking system to achieve precise tracking of the sun's movement.

The FTIR optical system comprises the HE-NE laser interferometric path and the sunlight interferometric path. Both sets of paths share the core interferometric system, with the laser and sunlight traveling along coaxial paths. The sunlight interferometric optical path primarily consists of a parabolic mirror F, which converts the sunlight imported from the solar tracking system into a set of parallel light. This parallel light is then divided into two perpendicular beams by a beam splitter O. One of these beams is reflected upward by a fixed mirror G. The upward-reflected light is then redirected by the beam splitter O towards another fixed mirror and subsequently gathered onto the infrared detector through a reflector J, along with the other beam that passes through a moving mirror and returns to the beam splitter for final redirection. Meanwhile, the HE-NE laser interferometric path mainly consists of the laser light source, which passes through a quasi-diameter element E into the same interferometric path as the sunlight. This laser light is then gathered onto the laser detector through a reflector K. The HE-NE laser signal detection and processing system primarily involves a four-quadrant silicon PIN photodiode for detecting the interference of the laser signal. After amplification, filtering, and shaping, the processed signal is input

into an FPGA for controlling the motion of moving mirrors and the attitude of fixed mirrors, as well as triggering the sampling of infrared interference signals.

The interference data acquisition and processing system primarily amplifies and filters the signals detected by the infrared detector. The interferogram is obtained through analog-to-digital (A/D) sampling and correction processes, which will constitute an important part of our testing. Spectral recovery, screening, inversion, and quantitative analysis of the interferograms are primarily conducted on a personal computer (PC).

4.2. CO_2 Observations and Analyses

In Fourier-transform spectroscopy, spectral information in the frequency domain is obtained from the time-domain output signal derived from the measurement. Therefore, once the acquisition and recovery of the interferogram are completed, the interferogram undergoes preprocessing steps such as phase correction, and subsequently, the spectrogram is obtained through FFT recovery. Figure 12 illustrates the process from the interferogram to the acquisition of the spectrogram for the ground-based FTIR spectrometer used to measure the solar spectrum.
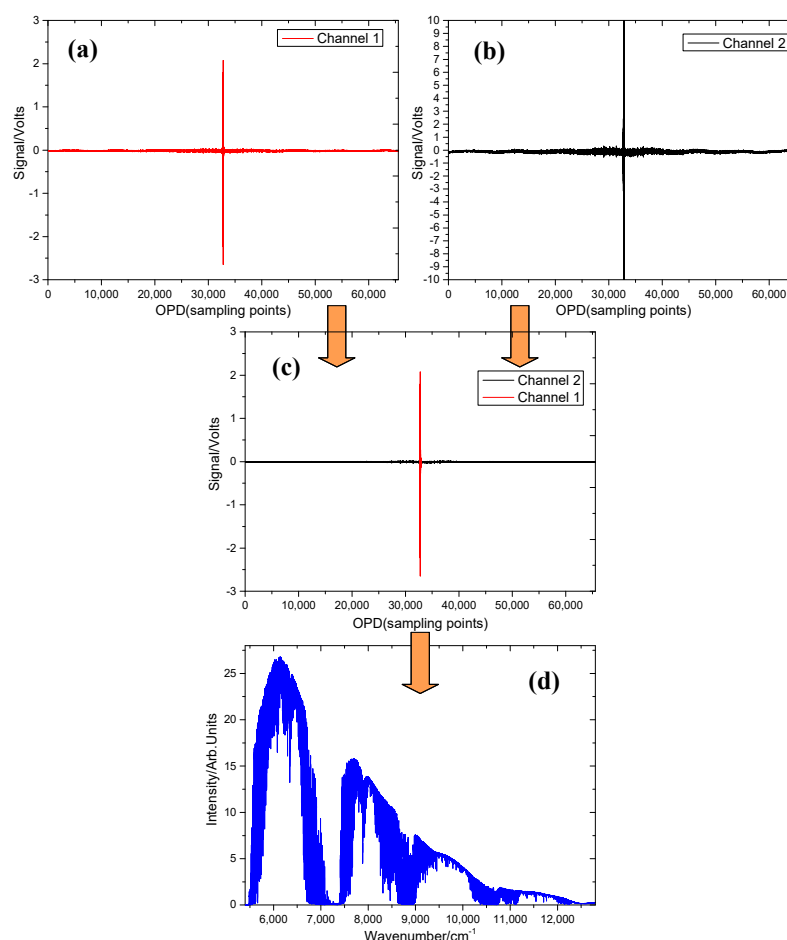

Figure 12. Interferogram acquisition to spectral recovery in field tests: (**a**) channel I; (**b**) channel II; (**c**) reconstructed interferogram; (**d**) spectrogram.

In the field of spectroscopy, Fourier-transform spectroscopy employs the time-domain output signal acquired from measurements. After undergoing mathematical transformation, we can extract the frequency-domain spectral information concealed within, thereby enabling an in-depth investigation of matter's properties. To obtain useful spectral information from the interferogram, a series of preprocessing steps must first be carried out, of which phase correction is a vital component. During the actual measurement process,

various factors (such as instrumental errors, environmental interference, etc.) may cause shifts in the interferogram's phase. If left uncorrected, these shifts will directly compromise the accuracy of the final spectral map. Therefore, adjusting the interferogram's phase using precise mathematical algorithms to align with the actual physical process is crucial for ensuring the quality of spectral analysis.

To eliminate this phenomenon, the phase can be corrected using a correction term. In Fourier-transform infrared spectroscopy theory [15], the interferogram can be expressed as:

$$I(\delta) = \int_0^\infty I_0(v) \cdot cos2\pi v\delta \, dv \tag{3}$$

Since $\varnothing\left(\widetilde{v}\right) = -\varnothing\left(-\widetilde{v}\right)$, Equation (3) can be expressed as:

$$B'\left(\widetilde{v}\right) = \int_{-\infty}^\infty I'(v)e^{-i2\pi\widetilde{v}x+i\varnothing(\widetilde{v})}dx = B_{real}\left(\widetilde{v}\right) + iB_{imag}\left(\widetilde{v}\right) \tag{4}$$

where $B_{real}\left(\widetilde{v}\right)$ and $B_{imag}\left(\widetilde{v}\right)$ are the real and imaginary parts.

The correction term $\varnothing\left(\widetilde{v}\right)$ can be calculated by having Equation (4):

$$\varnothing\left(\widetilde{v}\right) = \tan^{-1}\left(\frac{B_{imag}\left(\widetilde{v}\right)}{B_{real}\left(\widetilde{v}\right)}\right) \tag{5}$$

Combining Equations (4) and (5) above, an expression for the calibration spectrum can be obtained:

$$B'\left(\widetilde{v}\right) = B\left(\widetilde{v}\right)e^{i\varnothing(\widetilde{v})} \tag{6}$$

After phase correction and other preprocessing steps, the next stage involves using the fast Fourier transform (FFT) to obtain the spectral map. The FFT can efficiently transform a vast number of data in a short time, significantly enhancing the efficiency and accuracy of spectral analysis. In this process, every detail in the interferogram is meticulously analyzed and transformed into clearly discernible spectral lines on the spectral map, each corresponding to the characteristic absorption or emission of a specific component or structure within the material.

Figure 12 depicts the transition from an interferogram to a spectrogram. A raw interferogram, magnified by a factor of 1, is utilized as the data input for ADC channel one (Figure 12a). Similarly, another raw interferogram, magnified by a factor of 8, serves as the data input for ADC channel two (Figure 12b). After dividing all the data points on the combined two-channel interferogram by their respective gain magnifications, the recovered interferogram is created by selecting the 28/2 data points around the zero-phase difference (ZPD) of channel 1's interferogram and incorporating all data from channel 2, excluding the overlapping data points from channel 1. This composite forms the final recovered interferogram (Figure 12c). It is evident that the dual-channel ADC acquires and processes the interferogram to produce a complete version, which undergoes preprocessing and FFT recovery before being converted into a spectrogram (Figure 12d).

We tested the algorithm by comparing the concentrations of CO_2 columns derived from spectra. These spectra were acquired from interferograms: some using a single channel and others using two channels. The test weather conditions were clear and cloudless. Since there are no perfect data that are completely unaffected by clouds or changes in light intensity, and since the measured gas column may be higher than the true atmospheric column, we selected data where the change in solar radiation intensity during a single scan was within 5%. On 9 October 2024, in Hefei, China (longitude 117.096386°, latitude

31.867071°), we retrieved CO_2 column concentrations from FTIR spectra measured on the roof of Science Island.

Due to Science Island's location in the center of the lake, we anticipated minimal diurnal variation in CO_2. A nearly constant CO_2 column concentration was obtained from the measurement data using a two-channel interferometric data acquisition method. This contrasts with the control data, where the dispersion of the acquired CO_2 column concentration increases when the interferometric data are acquired using the conventional method. According to the results presented in Figure 13, for the complete dataset of 487 control measurements taken between 9:24:37 and 15:28:24 on the same day, the mean CO_2 column concentration of the data acquired using the conventional method was 426.1 ppm, with fluctuations ranging from 422.0 to 430.9 ppm. The mean CO_2 column concentration of the data acquired using the dual-channel interferometric method was 426.2 ppm, with fluctuations ranging from 424.4 to 427.8 ppm.
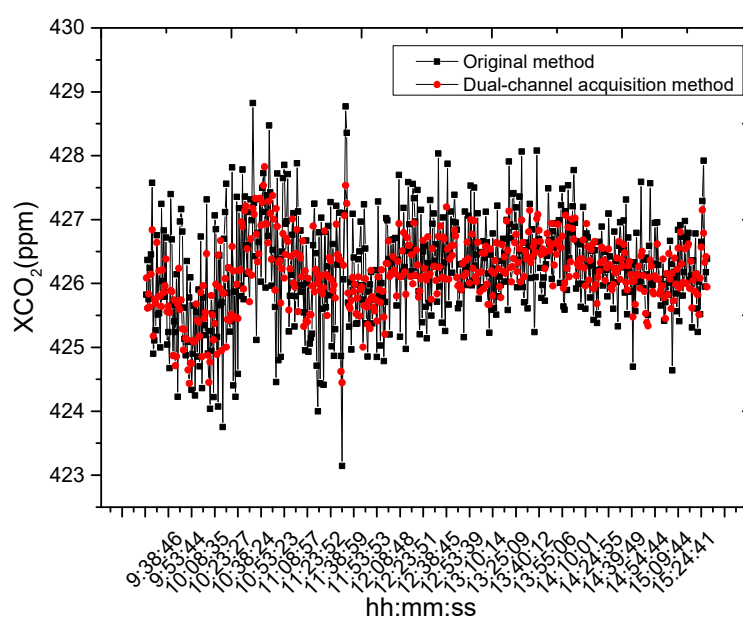

Figure 13. CO_2 column-concentration observation results.

In order to determine whether the dual-channel interferometric data acquisition method introduces bias into the gas retrieval process, we analyzed the degree of data deviation depicted in Figure 13. Across 487 measurements, the mean difference in CO_2 column concentration for data acquired using the traditional method was 0.9 ppm, with a standard deviation of 1.1 ppm. In contrast, the mean difference for data acquired using the dual-channel interferometric method was 0.4 ppm, with a standard deviation of 0.5 ppm.

Since it is difficult to simulate the real ambient atmosphere in vertical column-concentration measurements, to further demonstrate the repeatability and reliability of the CO_2 column-concentration measurement results, the ratio of the standard deviation to the daily average was employed to illustrate the variation relationship among data measured repeatedly on the same day. In 487 measurements, the accuracy of the CO_2 column concentration, as measured by the traditional method, was 0.27%. The accuracy of the CO_2 column concentration measured using the two-channel interferometric data acquisition method was 0.13%. The accuracy of the CO_2 column concentration was calculated using the following formula:

$$Gas_{precision} = \frac{\sigma}{\langle Gas \rangle} \times 100\% \tag{7}$$

Here, $Gas_{precision}$ represents the measurement precision of the gas to be measured, σ is the standard deviation of the time series, and $\langle Gas \rangle$ indicates the mean value of the measurement results.

5. Conclusions

In this paper, we propose a dual-channel ADC acquisition method for interferometric data acquisition in a ground-based Fourier-Transform Infrared (FTIR) greenhouse gas spectrometer. This method involves acquiring interferometric data through two ADC acquisition channels with different gains: the low-gain ADC channel primarily captures data near the zero optical-path difference (ZPD) spike, while the high-gain ADC channel focuses on acquiring small signals on the two flanks of the interferogram. Simulation verification results indicate that the signal-to-noise ratio is improved by a factor of 1.23. Additionally, the retrieval accuracy of CO_2 column concentration data is enhanced by a factor of 2.096, based on observations at a fixed point. We anticipate that this interferometric data acquisition method will have an increasingly significant impact on the selection of data acquisition techniques for FTIR spectrometers, particularly when the need to improve the accuracy of weak signals on the flanks of interferograms becomes more prominent, especially with limited ADC accuracy and dynamic range. In the future, we plan to continue applying this method to interferogram acquisition using a 24-bit synchronous ADC to further enhance instrument performance.

Author Contributions: Conceptualization, Y.D. and L.X.; formal analysis, Y.D. and L.X.; funding acquisition, L.J. and Y.S.; investigation, L.X.; methodology, Y.D.; resources, J.L. and W.L.; software, Y.D., L.Z., Y.S. and J.L.; validation, L.Z.; writing—original draft, Y.D.; writing—review and editing, Y.D. and L.X. All authors have read and agreed to the published version of the manuscript.

Institutional Review Board Statement: Not applicable.

Informed Consent Statement: Not applicable.

Data Availability Statement: The data underlying the results presented in this paper are not publicly available at this time, but may be obtained from the authors upon reasonable request.

Conflicts of Interest: The authors declare no conflicts of interest.

References

1. Löw, B.A.; Kleinschek, R.; Enders, V.; Sander, S.P.; Pongetti, T.J.; Schmitt, T.D.; Hase, F.; Kostinek, J.; Butz, A. A portable reflected-sunlight spectrometer for CO_2 and CH_4. *Atmos. Meas. Tech.* **2023**, *16*, 5125–5144. [CrossRef]
2. Humpage, N.; Boesch, H.; Okello, W.; Chen, J.; Dietrich, F.; Lunt, M.F.; Feng, L.; Palmer, P.I.; Hase, F. Greenhouse gas column observations from a portable spectrometer in Uganda. *Atmos. Meas. Tech. Discuss.* **2023**, *2023*, 5679–5707. [CrossRef]
3. Mostafavi Pak, N.; Hedelius, J.K.; Roche, S.; Cunningham, L.; Baier, B.; Sweeney, C.; Roehl, C.; Laughner, J.; Toon, G.; Wennberg, P.; et al. Using portable low-resolution spectrometers to evaluate Total Carbon Column Observing Network (TCCON) biases in North America. *Atmos. Meas. Tech.* **2023**, *16*, 1239–1261. [CrossRef]
4. Davis, S.P.; Abrams, M.C.; Brault, J.W. *Fourier Transform Spectrometry*; Academic Press: Cambridge, MA, USA, 2001.
5. Duan, M.; Zong, Y.; Zhu, R.; Li, J. Phase-tilt iteration: Accurate and robust phase extraction from random tilt-shift interferograms. *Opt. Lasers Eng.* **2021**, *142*, 106595. [CrossRef]
6. Shu, S.; Liu, J.; Xu, L.; Wang, Y.; Deng, Y.; Sun, Y. Real-Time Simulation of Clear Sky Background Radiation in Gas Infrared Remote Sensing Monitoring. *Photonics* **2024**, *11*, 904. [CrossRef]
7. Palchetti, L.; Lastrucci, D. Spectral noise due to sampling errors in Fourier-transform spectroscopy. *Appl. Opt.* **2001**, *40*, 3235–3243. [CrossRef]

8. Griffiths, P.R.; de Haseth, J.A. *Fourier Transform Infrared Spectrometry*, 2nd ed.; Analytical and Bioanalytical Chemistry; Springer: Berlin/Heidelberg, Germany, 2008; Volume 391, pp. 2379–2380.

9. Cohen, D.L. Performance degradation of a Michelson interferometer due to random sampling errors. *Appl. Opt.* **1999**, *38*, 139–151. [CrossRef] [PubMed]

10. Simon, A.; Metz, W.; Keens, A. Data acquisition and interferogram data treatment in FT-IR spectrometers. *Vib. Spectrosc.* **2002**, *29*, 97–101. [CrossRef]

11. Alber, G.M.; Marshall, A.G. Effect of sampling rate on Fourier transform spectra: Oversampling is overrated. *Appl. Spectrosc.* **1990**, *44*, 1111–1116. [CrossRef]

12. Brault, J.W. New approach to high-precision Fourier transform spectrometer design. *Appl. Opt.* **1996**, *35*, 2891–2896. [CrossRef] [PubMed]

13. Kang, Y. Analysis of sampling error in FTIR. In Proceedings of the PIAGENG 2013: Image Processing and Photonics for Agricultural Engineering, Sanya, China, 27–28 January 2013; SPIE: Bellingham, WA, USA, 2013; Volume 8761, pp. 122–127.

14. Hao, J.; Lu, C.; Jiang, W. Research on interference signal acquisition technology of Fourier transform infrared spectrometer. *Autom. Technol. Appl.* **2016**, *10*, 23–27.

15. Griffiths, P.R. Fourier transform infrared spectrometry. *Science* **1983**, *222*, 297–302. [CrossRef] [PubMed]

16. Kester, W. (Ed.) *Practical Design Techniques for Power and Thermal Management*; Analog Devices: Wilmington, MA, USA, 1998.